

# Spin-Boson Model to Demonstrate Quantum Tunneling in Biomolecules using IBM Quantum Computer

Yugojyoti Mohanta<sup>1\*</sup>, Dhurjati Sai Abhishikth<sup>2†</sup>, Kuruva Pruthvi<sup>2‡</sup>, Vijay Kumar<sup>3§</sup>, Bikash K. Behera<sup>3¶</sup> & Prasanta K. Panigrahi<sup>3||\*\*</sup>

<sup>1</sup>*Department of Physical Sciences, Indian Institute of Science Education and Research Berhampur, Ganjam, 760010, Odisha, India.*

<sup>2</sup>*Department of Physical Sciences, Indian Institute of Science Education and Research Thiruvananthapuram, Vithura, 695551, Kerala, India.*

<sup>3</sup>*Department of Physical Sciences, Indian Institute of Science Education and Research Kolkata, Mohanpur, 741246, West Bengal, India.*

**Efficient simulation of quantum mechanical problems can be performed in a quantum computer where the interactions of qubits lead to the realization of various problems possessing quantum nature. Spin-Boson Model (SBM) is one of the striking models in quantum physics that enables to describe the dynamics of most of the two-level quantum systems through the bath of harmonic oscillators. Here we simulate the SBM and illustrate its applications in a biological system by designing appropriate quantum circuits for the Hamiltonian of photo-synthetic reaction centers in IBM's 5-qubit quantum computer. We consider both two-level**

---

\*E-mail: yugojyoti16@iiserbpr.ac.in

†E-mail: dabhishikth2717@iisertvm.ac.in

‡E-mail: pruthvikuruva17@iisertvm.ac.in

§E-mail: vk13ms149@iiserkol.ac.in

¶E-mail: bkb13ms061@iiserkol.ac.in

||Corresponding author.

\*\*E-mail: pprasanta@iiserkol.ac.in

**and four-level biomolecular quantum systems to observe the effect of quantum tunnelling in the reaction dynamics. We study the behaviour of tunneling by changing different parameters in the Hamiltonian of the system. The results of SBM can be applied to various two-, four- and multi-level quantum systems explicating electron transfer process.**

## **1 Introduction**

Quantum computers have proved their superior power over classical ones while solving certain problems <sup>1-6</sup> among which simulation of the quantum systems has been a special attraction due to the exponential improvement in speeds and computational resources. Efficient simulation of quantum systems <sup>7-14</sup> has played a major role in motivating scientists coming up with the idea of a quantum computer <sup>3</sup>. The field of simulation of quantum mechanical problems in a quantum computer is progressing very fast and it has applications in many scientific branches like many-body theory <sup>15-18</sup>, condensed matter <sup>19,20</sup>, spin models <sup>21,22</sup>, quantum phase transitions <sup>23,24</sup>, quantum chemistry <sup>25</sup>, quantum chaos <sup>26</sup>, interferometry <sup>27-29</sup> and so on. Simulation by a quantum computer has been found to be more effective than simulated it in a classical computer <sup>30</sup>.

One of the most fundamental models of open quantum systems is the Spin-Boson Model (SBM) <sup>31,32</sup>, which comprises a two-level system and a large number of quantum harmonic oscillators linearly coupled to it and acting as the environment <sup>33</sup>. The influence of these degrees of freedom on the dynamics of the spin can be computed from the strength of the couplings between the spin, each oscillating mode and the frequency of the modes <sup>34-38</sup>. Though exact solution of the spin-boson model is not possible <sup>39</sup>, various simulation techniques such as real time quantum

Monte Carlo simulations<sup>40</sup> and exact Monte Carlo simulations<sup>41</sup> and approximation methods such as Noninteracting-blip approximation<sup>42</sup> and Bloch-Redfield equation have been extensively used to study the dynamics of this model. While most of the simulation performed in classical systems neglects the tunneling part<sup>37</sup>, through simulation of SBM on a quantum computer, we can obtain insightful results by incorporating the tunneling part in the Hamiltonian of the quantum system.

Here we apply the SBM to explain the dynamics of biomolecules in the photosynthetic reaction center, i.e. electron transfer reaction in *Rhodospseudomonas viridis*<sup>37,43,44</sup> and further extend this model to a four-level system. We study the time evolution of the given system from reactant state to product and from product to reactant state for different tunnelling parameters in such biological system at normal room temperature. We use IBM's quantum computer, 'IBM 5 Tenerife' (ibmqx4) to simulate the Hamiltonian of this systems, where many research problems have already been tackled<sup>45-74</sup>. The architecture of the 5-qubit chip 'ibmqx4' is discussed in Methods Section 4.

## 2 Results

**Two-Level System** The Hamiltonian of Spin-Boson Model for a two-level system is given by<sup>33,42</sup>,

$$\mathcal{H} = -\frac{\hbar\Delta\hat{\sigma}_x}{2} + \frac{\epsilon\hat{\sigma}_z}{2} + \frac{q\hat{\sigma}_x\sum c_\alpha x_\alpha}{2\hbar} + \sum \hbar w_\alpha \hat{b}_\alpha^\dagger \hat{b}_\alpha \quad (1)$$

where  $\hat{\sigma}_x$  and  $\hat{\sigma}_z$  are Pauli operators,  $\epsilon$  represents the energy difference between two states,  $\hbar$  represents the reduced Plank's constant,  $\Delta$  represents the hopping rate,  $q$  represents the protein conformation for initial state and  $c_\alpha$  describes the strength of the coupling of the electron transfer to the  $\alpha$  th oscillator and  $\hat{b}^\dagger, \hat{b}$  are bosonic creation and annihilation operators and tunnelling parameter is given by  $\frac{\hbar\Delta}{2}$ .

Here we apply the Spin-Boson (SB) Hamiltonian to a two-level biological system which is similar to *Rhodospseudomonas viridis*'s photosynthetic reaction center<sup>37,75</sup>. The system can be visualised using a Marcus energy diagram (Fig. 1 A) which consists of two potential wells with the energy difference  $\epsilon$ . The distance between the two potentials is denoted as  $q$  which is so called protein conformation.  $E_R$  and  $E_P$  are the two energies of the reactant and product states, where  $\epsilon = E_R - E_P$ .

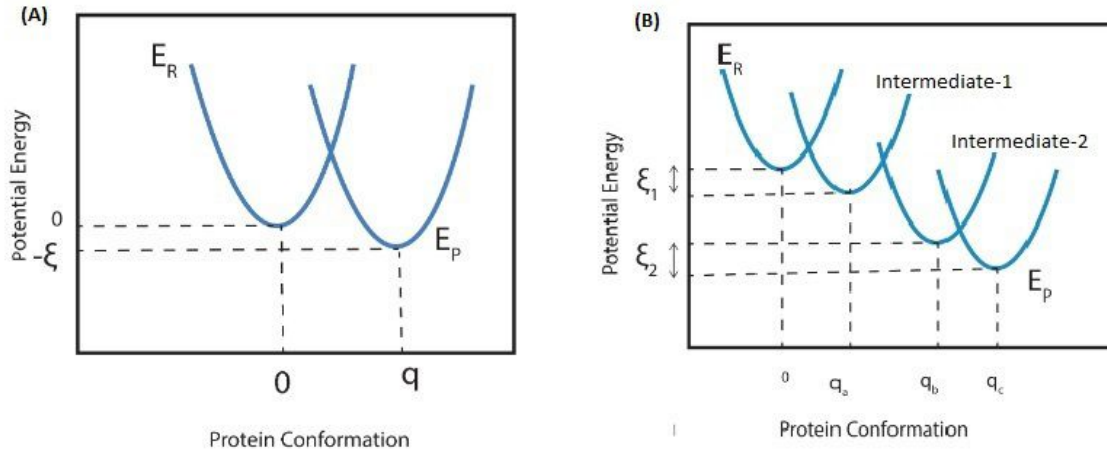


Figure 1: **Marcus diagram for two-level and four-level systems.** **Case A:**  $E_R$  and  $E_P$  represent the energies of reactant and product respectively,  $\epsilon$  is the energy difference between reactant and product, and  $q$  is the protein conformation of the product. **Case B:**  $E_R$  and  $E_P$  represent the energies of reactant and product respectively. Intermediate-1 and Intermediate-2 are the two intermediate states of the reaction.  $\epsilon_1$  is the energy difference between reactant and intermediate-1 state and  $\epsilon_2$  is the energy difference between intermediate-2 and the product state.  $q_a$ ,  $q_b$  and  $q_c$  are the protein conformation of intermediate-1, intermediate-2 and the product respectively.

**Four-Level System** The Spin-Boson Hamiltonian can be extended to a four-level system which describes electron transfer methods in four-level photosynthetic reaction. This is done by adding two intermediate energy states in between reactant state and product state. The system can be represented using a Marcus energy diagram Fig. as illustrated in Fig. 1 **B**. To simplify the system we model the Hamiltonian in such a way that tunnelling is only allowed in between reactant state

( $E_R$ ) and Intermediate-1 and in between Intermediate-2 and product state ( $E_P$ ).  $\epsilon_1$  and  $\epsilon_2$  denote the energy differences between the reactant and Intermediate-1, and the Intermediate-2 and product state respectively.

The Hamiltonian describing the four-level system is given by <sup>33,76</sup>,

$$\mathcal{H} = -\frac{\hbar\Delta_1\hat{\sigma}_x^1}{2} + \frac{\epsilon_1\hat{\sigma}_z^1}{2} + \frac{q\hat{\sigma}_x^1\sum c_\alpha x_\alpha}{2\hbar} + \sum \hbar w_\alpha \hat{a}_\alpha^\dagger \hat{a}_\alpha - \frac{\hbar\Delta_2\hat{\sigma}_x^2}{2} + \frac{\epsilon_2\hat{\sigma}_z^2}{2} + \frac{q\hat{\sigma}_x^2\sum c_\beta x_\beta}{2\hbar} + \sum \hbar w_\beta \hat{b}_\beta^\dagger \hat{b}_\beta + J_{12}(\hat{\sigma}_x^1\hat{\sigma}_x^2 + \hat{\sigma}_y^1\hat{\sigma}_y^2) \quad (2)$$

where  $\hat{\sigma}_x^i$  and  $\hat{\sigma}_z^i$  are the Pauli operators acting on the  $i$ th qubit,  $\epsilon_1$  and  $\epsilon_2$  are the energy differences between the states,  $\hbar$  is the reduced Plank's constant,  $\Delta_1$  and  $\Delta_2$  represent the hopping rates between two energy states,  $q$  is the distance between two wells, and  $c_\alpha$  and  $c_\beta$  describe the strength of the coupling of the electron transfer to the  $\alpha$ th and  $\beta$ th oscillator respectively. Here  $\hat{a}^\dagger$  and  $\hat{b}^\dagger$  are the bosonic creation operators,  $\hat{a}$  and  $\hat{b}$  are the annihilation operators, and  $J_{12}$  is the coupling constant between the two qubits <sup>76-78</sup>.

The reaction dynamics of photosynthetic reaction center (i.e., the conversion of reactant to product state) and the tunnelling effect <sup>79</sup> in two-level and four-level system is studied by making appropriate quantum circuit. The Hamiltonian for the system is simulated using IBM'S five-qubit quantum computer for different instances of time ( $t$ ). To understand the quantum tunnelling efficiently, we took the values of hopping rates ( $\Delta_1, \Delta_2$ ), energy differences ( $\epsilon_1, \epsilon_2$ ) to be equal for both of the qubits in the four-level system and took approximate values for the terms containing

summation. The executions and graphs are shown in Results Section 2.

**Quantum Circuits** For the two-level and the four-level system, the design of the circuit of the SB Hamiltonian is given Figs. 2 & 3. The values of all the parameters in the Hamiltonian are discussed in Methods Section 4. The Hamiltonian is executed in quantum computer and the formation of product of the reaction is observed and the probability of formation is plotted against time for different tunnelling matrix elements. We observed changes in electron transfer rate as the tunnelling parameter or the value of tunneling matrix element varies in the Hamiltonian. The tunnelling effect can be observed as the reactant forming the product and vice-versa. We plotted a bar graph for time evolution containing states of both the systems (two-level and four-level) with their probabilities. The quantum circuits for two-level are shown in Fig. 2.

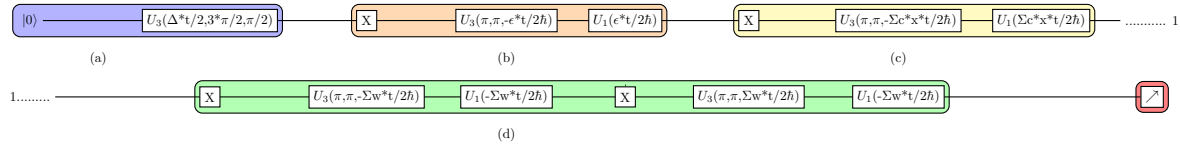


Figure 2: **Circuit diagram for two-level system Hamiltonian.** (a) represents the tunneling term ( $\frac{\hbar\Delta}{2}$ ), (b) represents the energy difference ( $\epsilon$ ), (c) represents the coupling between system and bath and (d) represents the bath term.

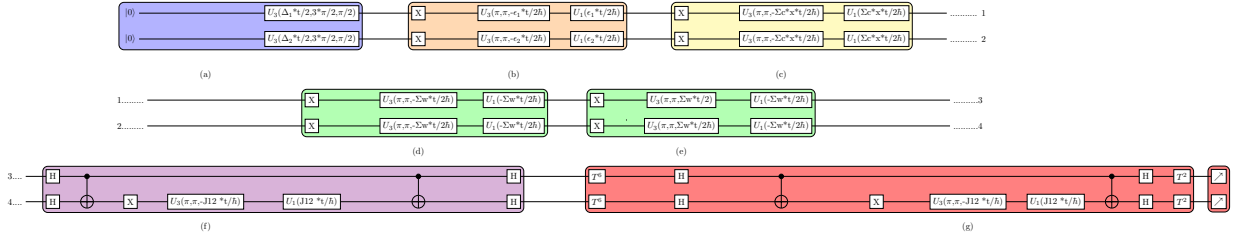
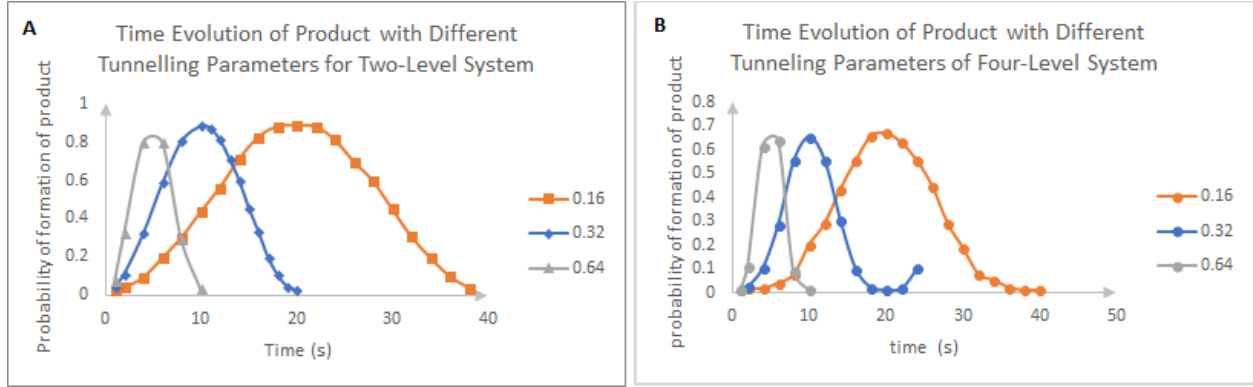


Figure 3: **Circuit diagram for four-level system Hamiltonian.** (a) represents the tunnelling terms ( $\frac{\hbar\Delta_1}{2}$ ) and ( $\frac{\hbar\Delta_2}{2}$ ). (b) represents the energy difference between two states  $\epsilon_1$  and  $\epsilon_2$ . (c) represents the coupling with the bath, (d) & (e) represent the bath term for each qubit respectively, (e) & (f) represent the coupling term between 2-qubits.

Tunnelling of reaction state into product state and vice-versa can be visualised in Fig. 4 as the time (t) evolves. It is observed that the time taken for tunneling from reaction state to product state is approximately decreases by half as the tunnelling parameter doubles.





**Figure 4: Time evolution of product of two-level and four-level system.** Case A: Time evolution of product with change in tunneling matrix ( $\frac{\hbar\Delta}{2}$ ) of two-level system describing photosynthetic reaction center. We evolve the system by increasing time till significant tunnelling is observed from the reactant state to the product state and vice-versa. The graphs were plotted for three different tunnelling parameters (orange graph is for  $0.16 \times 10^{-22} J$ , blue for  $0.32 \times 10^{-22} J$  and grey for  $0.64 \times 10^{-22} J$ ) and time shown in graph is in order of  $10^{-12} s$ . We can clearly infer that the time taken for tunnelling decreases or the tunnelling rate increases as the tunnelling parameter increases. Initially, the product state  $|1\rangle$  has 0 probability and reactant state  $|0\rangle$  have probability 1, then slowly as time evolves the probability of formation of the product reaches 1 and reactant state 0. After further time evolution, the products get tunnel back to the reactant state which is referred as tunneling cycle. **Case B:** For two qubit system the product state ( $|11\rangle$ ), intermediate states ( $|01\rangle$ ) and ( $|10\rangle$ ) have 0 probability and reactant state ( $|00\rangle$ ) have probability 1, then slowly as time evolves the probability of formation of the product reaches 1 and reactant state probability falls to 0.

the initial configuration of the two-level system illustrating electron transfer in photosynthetic reaction center is taken such that reactant state has a probability of 1 and product state has a probability of 0. As the time evolves in the system, concentration of product increases and concentration of reactant decreases. For tunnelling parameter  $0.16 \times 10^{-22} J$ , it reaches nearly equilibrium stage (i.e., the concentration of product state and reaction state are equal) at time  $t=11 \times 10^{-12}s$ . On further evolving the system, the probability of product state nearly reaches 1 and reactant state reaches 0, at about  $t=22 \times 10^{-12}s$ . After then, the system is further evolved and the tunnelling takes place in the reverse direction, i.e., the product gets tunnel back to the reactant state. This can be considered as tunnelling cycle and the systems with tunnelling parameters  $0.16 \times 10^{-22} J$ ,  $0.32 \times 10^{-22} J$  and  $0.64 \times 10^{-22} J$  take about  $40 \times 10^{-12}s$ ,  $20 \times 10^{-12}s$ ,  $10 \times 10^{-12}s$  respectively for one full tunnelling cycle.

In the four-level system describing photosynthetic reaction center, initially, the reactant has a probability of 1 and Intermediate-1, Intermediate-2, and the product state have a probability 0. As we evolve the system with time, the reactant state gets tunnelled into Intermediate-1 state ( $|01\rangle$ ), and as the reaction progresses  $|01\rangle$  gets converted to  $|10\rangle$ , and  $|10\rangle$  state tunnels in the product state ( $|11\rangle$ ). For the system with tunnelling parameter  $0.16 \times 10^{-22} J$ , we reach equilibrium at  $t=14 \times 10^{-12}$ . At  $t = 22 \times 10^{-12}s$ , the product state has a probability of 1, and all other states have probability 0 and the system returns to the initial condition. This phenomena can be here referred as tunneling cycle as the reactant state tunnels to the product state and the product state then tunnels back to the reactant state.

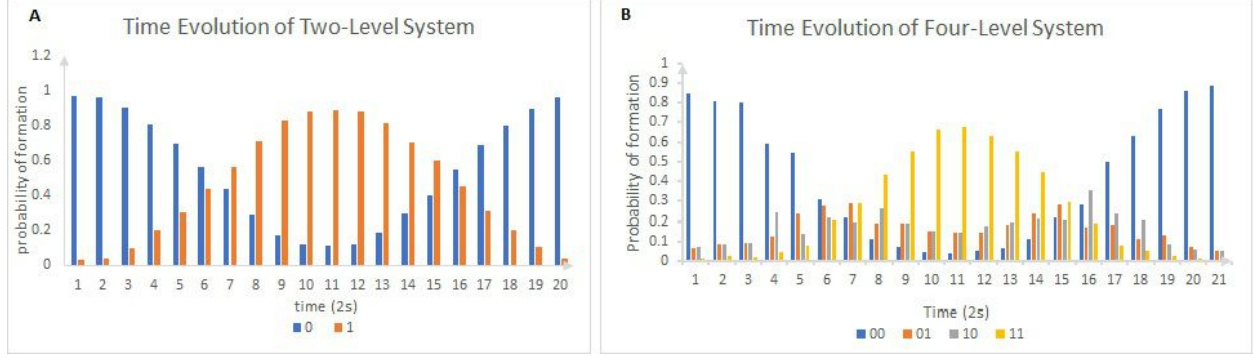


Figure 5: **Bar graph for time evolution of reactants, products and intermediate states.** Case A : Bar graph showing the probability of formation of reactant and product of a two-level system as the time evolves at tunnelling parameter  $= 0.16 \times 10^{-22} J$ .  $|0\rangle$  state is the reactant state shown in blue and  $|1\rangle$  state is the product state in orange. **Case B:** Bar graph showing the probability of formation of reactant and product of a four-level system as the time evolves at tunnelling parameter  $= 0.16 \times 10^{-22} J$ . The four colours blue, orange, grey and yellow represent the reactant ( $|00\rangle$ ), Intermediate-1 ( $|01\rangle$ ), Intermediate-2 ( $|10\rangle$ ) and the product ( $|11\rangle$ ) state respectively. In both **Cases A and B** the time taken is in order of  $10^{-12} s$ .

Fig. 6 gives a grasp on how tunnelling parameter affects the formation of the product, and we can see that the reactant is getting tunnelled into the product at  $t=10^{-12} s$  as the tunnelling parameter  $(\frac{\hbar\Delta}{2})$  changes.

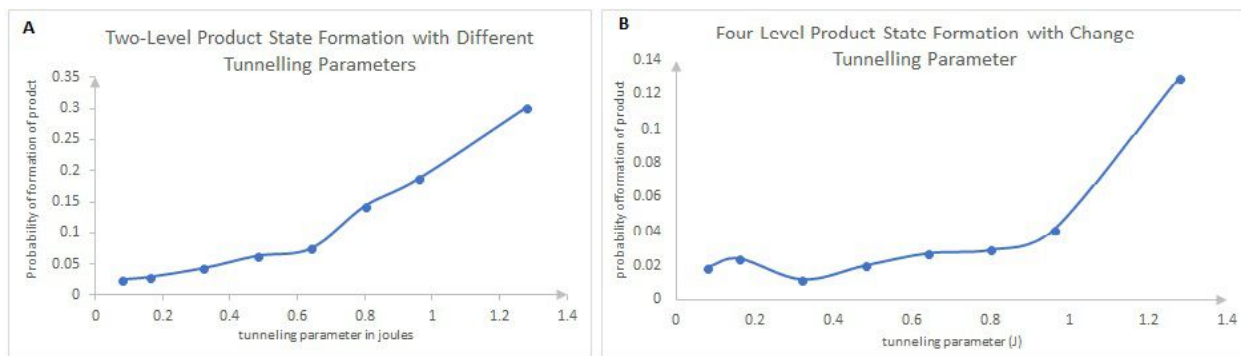


Figure 6: **Product formation with different tunnelling parameter. Case A:** Graph showing the changes in concentration of product when there is a change in tunnelling parameter at  $t = 10^{-12}$ s for the two-level system. We can observe that the concentration of product significantly increases with increase in tunneling parameter at a constant time. **Case B:** Graph showing the changes in the concentration of product when there is a change in tunnelling parameter at  $t = 10^{-12}$ s for four-level system. In both cases tunneling parameter is of order the  $10^{-22}$ .

### 3 Discussion

We have successfully demonstrated the effect of quantum tunnelling and studied the reaction dynamics of the biological system at normal room temperature consisting of two-level system and four-level system using spin-boson model. We studied how the system evolves for different tunneling parameters and found that rates of conversion of reactant to product increase with increase in

tunneling parameter values. Study of four level system can be improved by allowing the tunnelling in between all four states. This can be further analyzed by taking different tunneling values for each qubits and different coupling values in between qubits. System dynamics can be observed at different temperature conditions and at different reaction rates in the system. This model can be extended for more than four state electron transfer reaction consisting of multi-intermediate states. Similar model can be applied to simulate the dynamics of Fluorescence Resonance Energy Transfer <sup>76,77</sup>, Retinal in Rhodopsin environment and a quantum dot in a polar solvent <sup>76</sup>. The spin-boson model can be used for wide range of physical processes including electron transfer <sup>42,80,81</sup>, macroscopic quantum coherence <sup>82</sup> and hydrogen tunneling <sup>83</sup>.

#### 4 Methods

The values taken for simulating the above Hamiltonians are fixed for normal room temperature. The values of the following parameters are, tunnelling parameter ( $\frac{\hbar\Delta}{2}$ ) =  $3.2 \times 10^{-23} J$ ,  $q = 1$  <sup>37</sup>, energy difference ( $\epsilon$ ) =  $4.8 \times 10^{-20} J$ ,  $\sum c_\alpha x_\alpha \approx 7.484 \times 10^{-16} J$  <sup>37</sup> and  $\sum \omega_\alpha$  is  $1.1594 \times 10^{-16} J$  and number of harmonic oscillators <sup>37</sup> constitute the bath are taken as order of  $10^4$ . For the four-level system the above same values are taken for both the qubits and except the value of  $J_{12}$  which is taken as  $2.603 \times 10^{-16} J$  <sup>77,78</sup>.

**Simulation of Hamiltonian:** For simulation of the Hamiltonian <sup>84-86</sup> we use first order Trotter decomposition, which is given by,

$$e^{-i\mathcal{H}t} = e^{-i\mathcal{H}_1t} e^{-i\mathcal{H}_2t} \dots e^{-i\mathcal{H}_nt} + O(t^2) \quad (3)$$

where  $\mathcal{H}_1, \mathcal{H}_2, \dots, \mathcal{H}_n$  are Hamiltonians acting on local subsystems involving k-qubits of an n-qubit system. The system Hamiltonian can be written as,  $\mathcal{H} = \sum_1^n \mathcal{H}_k$ . Then the Hamiltonian is decomposed into a sequence of unitary transformations which can be implemented by using any set of universal quantum gates. In the above model, the Hamiltonian for a two state system is given by Eq. (1).

To implement the Trotter decomposition, we use  $\mathcal{H} = \mathcal{H}_1 + \mathcal{H}_2 + \mathcal{H}_3 + \mathcal{H}_4$ . Time evolution of quantum mechanical system is given by unitary transformation  $\hat{U}(t)$ , where

$$\hat{U}(t) = e^{\frac{-i\mathcal{H}t}{\hbar}} \quad (4)$$

Time evolution of  $\mathcal{H}_1$  is given by

$$e^{\frac{-i\mathcal{H}_1 t}{\hbar}} = e^{\frac{i\Delta\sigma_x t}{2}} \quad (5)$$

where  $\mathcal{H}_1 = -\frac{\hbar\Delta\sigma_x}{2}$ . which can be written in matrix form 
$$\begin{bmatrix} \cos \frac{\Delta t}{2} & i \sin \frac{\Delta t}{2} \\ i \sin \frac{\Delta t}{2} & \cos \frac{\Delta t}{2} \end{bmatrix}$$

The above matrix acts on a single qubit. Here t is the time elapsed since the beginning of the experiment. As the IBM Q Experience is a static system, by taking t as a controllable parameter we are able to effectively simulate the dynamics and time evolution of a two state biological system .

This matrix can be implemented on IBM Quantum Experience by using IBM's  $U3(\theta, \lambda, \phi)$ . This matrix can be written in term of  $U3(\theta, \lambda, \phi)$  by setting the parameters in the form  $U3(\frac{\Delta t}{2}, \frac{3\pi}{2}, \frac{\pi}{2})$ .

Similarly,  $\mathcal{H}_2, \mathcal{H}_3$  and  $\mathcal{H}_4$  can be implemented and quantum circuit for two-level system can

be designed by using  $U3(\theta, \lambda, \phi)$ ,  $U1(\theta)$  and X Gates as shown Fig. 2.

For four level system, which is given by Hamiltonian Eq. 2 and  $\mathcal{H}$  can be written as,

$$\mathcal{H} = \mathcal{H}_1 + \mathcal{H}_2 + \mathcal{H}_3 + \mathcal{H}_4 + \mathcal{H}_5 + \mathcal{H}_6 + \mathcal{H}_7 + \mathcal{H}_8 + \mathcal{H}_9$$

and  $\mathcal{H}_1$  takes the matrix form  $\begin{bmatrix} \cos \frac{\Delta_1 t}{2} & \iota \sin \frac{\Delta_1 t}{2} \\ \iota \sin \frac{\Delta_1 t}{2} & \cos \frac{\Delta_1 t}{2} \end{bmatrix}$  acting on the qubit 1 and identity on qubit 2.

Similarly,  $\mathcal{H}_2, \mathcal{H}_3, \mathcal{H}_4, \mathcal{H}_5, \mathcal{H}_6, \mathcal{H}_7, \mathcal{H}_8 \& \mathcal{H}_9$  can be implemented and quantum circuit for four level system can be designed by using  $U3(\theta, \lambda, \phi)$ ,  $U1(\theta)$ , X, H, T and CNOT Gates <sup>87</sup>, which is shown in Fig. 3.

**Experimental Architecture** The experimental device specification of IBM Q 5 Tenerife [ibmqx4] chip are shown in Table 1 <sup>88</sup>, the Fig. 7 depicts the connection and control of five qubits (Q0, Q1, Q2, Q3 and Q4). The single-qubit gate error is of the order  $10^{-3}$ . The multi-qubit and readout error are of the order  $10^{-2}$ . Randomized benchmarking is used to measure the gate errors.

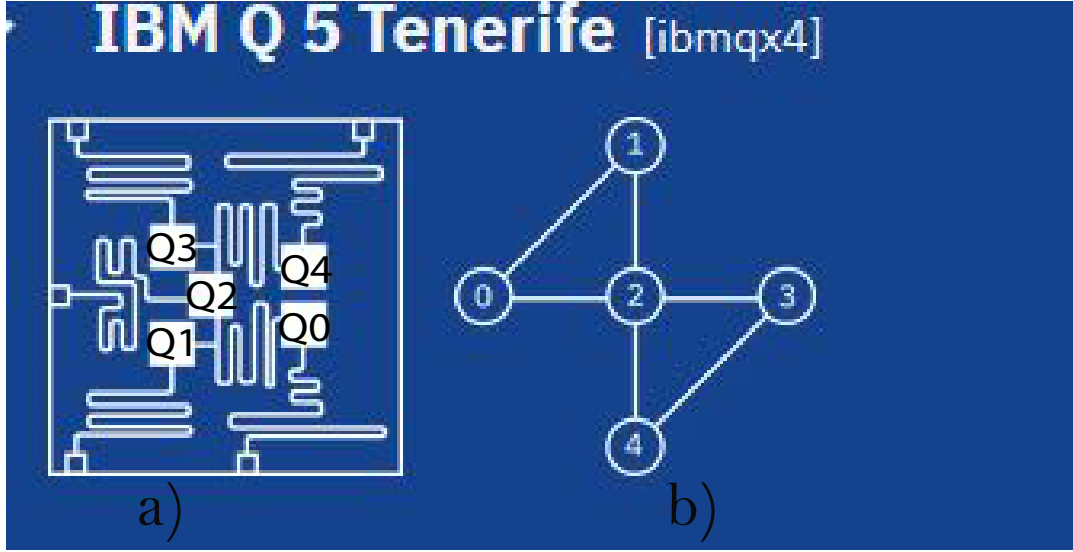


Figure 7: **Architecture of IBM Q5(a)** A picture shows the chip layout of 5-qubit quantum processor Tenerife [ibmqx4]. All 5 transmon qubits (Q0,Q1,Q2,Q3 and Q4) are connected with the two coplanar waveguide (CPW) resonators as shown. Qubits Q2, Q3 and Q4 are coupled by coplanar waveguide (CPW) resonators with resonances around 6.6 GHz, Qubits Q0, Q1 and Q2 are coupled by another coplanar waveguide (CPW) resonators with resonances around 7.0 GHz. Each qubit has a dedicated CPW for the control and readout. Two qubits gates are connected with a superconducting bus resonator. **(b)** The IBM Q experience uses the cross-resonance interaction as the basis for the CX-gate which is as follows:  $\{Q1 \rightarrow (Q0), Q2 \rightarrow (Q0, Q1, Q4), Q3 \rightarrow (Q2, Q4)\}$ , where  $i \rightarrow (j)$  means  $i$  and  $j$  denote the control qubit and the target qubit respectively for implementation of CNOT gate in the chip.



Qubits	$T_1^{\parallel} (\mu s)$	$T_2^{\perp} (\mu s)$	GE <sup>†</sup>	RE <sup>‡</sup>
Q0	50.80	13.90	0.77	6.40
Q1	56.30	57.70	1.63	6.10
Q2	42.00	49.90	1.20	6.00
Q3	33.10	15.30	3.01	11.00
Q4	52.30	26.20	0.94	5.68

$\parallel$  Relaxation time,  $\perp$  Coherence time,  $\dagger$  Gate Error,  $\ddagger$  Readout Error

Table 1: **Experimental parameters of the device ‘ibmqx4’ Tenerife.**

## References

1. Grover, L. K. Quantum Mechanics helps in searching for a needle in a haystack. *Phys. Rev. Lett.* **79**, 325 (1997).
2. Deutsch, D. & Jozsa, R. Rapid solutions of problems by quantum computation. *Proc. R. Soc. Lond. A* **439**, 553 (1992).
3. Feynman, R. P. Simulating physics with computers. *Int. J. Theor. Phys.* **21**, 467 (1982).
4. Childs, A.M. et al. Exponential algorithmic speedup by quantum walk. *Proceedings of the 35th ACM Symposium on Theory of Computing*, p. 59 (ACM Press, New York, 2003).
5. Simon, D. On the power of quantum computation. *Found. Comput. Sci. 1994 Proc. 35th Ann. Symp.*, pages 116–123 (1994)

6. Gerjuoy, E. Shor's factoring algorithm and modern cryptography. An illustration of the capabilities inherent in quantum computers. *Am. J. Phys.* **73**, 521–540 (2005).
7. Aspuru-Guzik, A., Duto, A. D., Love, P. J. & Head-Gordon, M. Simulated quantum computation of molecular energies. *Science* **309**, 5741 (2005).
8. Farhi, E. et al. A Quantum Adiabatic Evolution Algorithm Applied to Random Instances of an NP-Complete Problem. *Science* **292**, 472–475 (2001).
9. Han, K.-H. & Kim, J.-H. Genetic quantum algorithm and its application to combinatorial optimization problem. *Proc. CEC* **2**, 1354–1360 (2000).
10. Chuang, I. L., Vandersypen, L. M. K., Zhou, X., Leung, D. W. & Lloyd, S. Experimental realization of a quantum algorithm. *Nature* **393**, 143–146 (1998).
11. Jones, J. A., Mosca, M. & Hansen, R. H. Implementation of a quantum search algorithm on a quantum computer. *Nature* **393**, 344–346 (1998).
12. Gulde, S. et al. Implementation of the Deutsch-Jozsa algorithm on an ion-trap quantum computer. *Nature* **421**, 48–50 (2003).
13. Harrow, A. W., Hassidim, A. & Lloyd, S. Quantum Algorithm for Linear Systems of Equations. *Phys. Rev. Lett.* **103**, 150502 (2009).
14. Gerritsma, R. et al. Quantum simulation of the Dirac equation. *Nature* **463**, 68 (2010).
15. Tseng, C. H. et al. Quantum simulation of a three-body-interaction Hamiltonian on an NMR quantum computer. *Phys. Rev. A* **61**, 012302 (1999).

16. Negrevergne, C. et al. Liquid-state NMR simulations of quantum many-body problems. *Phys. Rev. A* **71**, 032344 (2005).
17. Peng, X. H., Zhang, J. F., Du, J. F. & Suter, D., Quantum simulation of a system with competing two- and three-body interactions. *Phys. Rev. Lett.* **103**, 140501 (2009).
18. Feng, G. R., Xu, G. F. & Long, G. L., Experimental realization of nonadiabatic holonomic quantum computation. *Phys. Rev. Lett.* **110**, 190501 (2013).
19. Edwards, E. E. et al. Quantum simulation and phase diagram of the transverse-field Ising model with three atomic spins. *Phys. Rev. B* **82**, 060412 (2010).
20. Zhang, J. F. et al. Direct observation of quantum criticality in Ising spin chains. *Phys. Rev. A* **79**, 012305 (2009).
21. Garcia-Ripoll, J. J., Martin-Delgado, M. A. & Cirac, J. I. Implementation of Spin Hamiltonians in Optical Lattices. *Phys. Rev. Lett.* **93**, 250405 (2004).
22. Lanyon, B. P. *et al.* Universal Digital Quantum Simulation with Trapped Ions. *Science* **332**, 57–61 (2011).
23. Greiner, M., Esslinger, T., Mandel, O., Hansch, T. W. & Bloch, I. Quantum phase transition from a superfluid to a Mott insulator in a gas of ultracold atoms. *Nature* **415**, 39–44 (2002).
24. Pollet, L., Picon, J. D., Buchler, H. P. & Troyer, M. Supersolid Phase with Cold Polar Molecules on a Triangular Lattice. *Phys. Rev. Lett.* **104**, 125302 (2010).

25. Lidar, D. A. & Wang, H. Calculating the thermal rate constant with exponential speedup on a quantum computer. *Phys. Rev. E* **59**, 2429 (1999).
26. Weinstein, Y. S., Lloyd, S., Emerson, J. & Cory, D. G. Experimental implementation of the quantum baker's map. *Phys. Rev. Lett.* **89**, 157902 (2002).
27. Leibfried, D. *et al.* Trapped-Ion Quantum Simulator: Experimental Application to Nonlinear Interferometers. *Phys. Rev. Lett.* **89**, 247901 (2002).
28. Viyuela, O. *et al.* Observation of topological Uhlmann phases with superconducting qubits. *npj Quantum Inf.* **4**, 10 (2018).
29. Langford, N. K. *et al.* Experimentally simulating the dynamics of quantum light and matter at deep-strong coupling. *Nat. Comm.* **8**, 1715 (2017).
30. Buluta, I. & Nori, F. Quantum Simulators. *Science* **326**, 5949 (2009).
31. Mascherpa, F., Smirne, A., Huelga, S. F., & Plenio, M. B. Open Systems with Error Bounds: Spin-Boson Model with Spectral Density Variations. *Phys. Rev. Lett.* **118**, 5 (2017).
32. Weiss, U. Quantum Dissipative Systems. *2nd edn. (World Scientific, 1999)*.
33. Leppakangas, J. *et al.* Quantum simulation of the spin-boson model with a microwave circuit. *Phys. Rev. A* **97**, 052321 (2018).
34. Schulten, K. & Tesch, M. Coupling of protein motion to electron transfer: Molecular dynamics and stochastic quantum mechanics study of photosynthetic reaction centres. *Chem. Phys.* **158**, 421–446 (1991).

35. Nonella, M. & Schulten, K. Molecular dynamics simulation of electron transfer in proteins. Theory and application to  $Q_A \rightarrow Q_B$  transfer in photosynthetic centre. *J. Phys. Chem.* **95**, 2059–2067 (1991)
36. Krishtalik, L. I. Fast electron in photosynthetic reaction centre: effect of time-evolution of dielectric response. *Biochim. Biophys. Acta Bioener.* **1228**, 58–66 (1995)
37. Xu, D. & Schulten, K. Coupling of protein motion to electron transfer in a photosynthetic reaction center: investigating the low temperature behavior in the framework of the spin-boson model. *Chem. Phys.* **182**, 91–117 (1994).
38. DeVault, D. Quantum-mechanical tunneling in biological systems. *Q. Rev. Biophys.* **13**, 387–564 (1980).
39. Reinhold, E. & Mak, C. H. Low-temperature dynamical simulation of spin-boson systems. *Phys. Rev. B* **50**, 15210 (1994).
40. Luck, A., Winterstetter, M., Weiss, U. & Mak, C. H. Quantum Monte Carlo simulations of driven spin-boson systems. *Phys. Rev. E* **58**, 5565 (1998).
41. Lee, C. K., Cao, J. & Gong, J. Noncanonical statistics of a spin-boson model: Theory and exact Monte Carlo simulations. *Phys. Rev. E* **86**, 021109 (2012).
42. Leggett, A. J., Chakravarty, S. A. T. Dorsey, Matthew P. A. Fisher, Anupam Garg, and W. Zwerger Dynamics of the dissipative two-state system . *Rev. Mod. Phys.* **59**, 1-85 (1987).

43. Kirmaier, C. & Holten, D. Primary photochemistry of reaction centers from the photosynthetic purple bacteria. *Photosynth. Res.* **13**, 225 (1987).
44. Hu, X. & Schulten, K. How Nature Harvests Sunlight?. *Phys. Today* **50**, 28 (1997).
45. García-Martín, D. & Sierra, G. Five Experimental Tests on the 5-Qubit IBM Quantum Computer. *arXiv preprint arXiv:1712.05642* (2017).
46. Das, S. & Paul, G. Experimental test of Hardy's paradox on a five-qubit quantum computer. *arXiv preprint arXiv:1712.04925* (2017).
47. Behera, B. K., Banerjee, A. & Panigrahi, P. K. Experimental realization of quantum cheque using a five-qubit quantum computer. *Quantum Inf. Process.* **16**, 312 (2017).
48. Hegade, N. N., Behera, B. K. & Panigrahi, P. K. Experimental Demonstration of Quantum Tunneling in IBM Quantum Computer. *arXiv preprint arXiv:1712.07326* (2017).
49. Majumder, A., Mohapatra, S. & Kumar, A. Experimental Realization of Secure Multiparty Quantum Summation Using Five-Qubit IBM Quantum Computer on Cloud. *arXiv preprint arXiv:1707.07460* (2017).
50. Sisodia, M., Shukla, A., Thapliyal, K. & Pathak, A. Design and experimental realization of an optimal scheme for teleportation of an n-qubit quantum state. *Quantum Inf. Process.* **16**, 292 (2017).

51. Dash, A., Rout, S., Behera, B. K. & Panigrahi, P. K. A Verification Algorithm and Its Application to Quantum Locker in IBM Quantum Computer. *arXiv preprint arXiv:1710.05196* (2017).
52. Wootton, J. R. Demonstrating non-Abelian braiding of surface code defects in a five qubit experiment. *Quantum Sci. Technol.* **2**, 015006 (2017).
53. Berta, M., Wehner, S. & Wilde, M. M. Entropic uncertainty and measurement reversibility. *New J. Phys.* **18**, 073004 (2016).
54. Deffner, S. Demonstration of entanglement assisted invariance on IBM's quantum experience. *Heliyon* **3**, e00444 (2016).
55. Huffman, E. & Mizel, A. Violation of noninvasive macrorealism by a superconducting qubit: Implementation of a Leggett-Garg test that addresses the clumsiness loophole. *Phys. Rev. A* **95**, 032131 (2017).
56. Alsina, D. & Latorre, J. I. Experimental test of Mermin inequalities on a five-qubit quantum computer. *Phys. Rev. A* **94**, 012314 (2016).
57. Yalçinkaya, İ. & Gedik, Z. Optimization and experimental realization of quantum permutation algorithm. *Phys. Rev. A* **96**, 062339 (2017).
58. Ghosh, D., Agarwal, P., Pandey, P., Behera, B. K. & Panigrahi, P. K. Automated Error Correction in IBM Quantum Computer and Explicit Generalization. *Quantum Inf. Process.* **17**, 153 (2018).

59. Kandala, A. *et al.* Hardware-efficient variational quantum eigensolver for small molecules and quantum magnets. *Nature* **549**, 242–246 (2017).
60. Alvarez-Rodriguez, U., Sanz, M., Lamata, L. & Solano, E. Quantum Artificial Life in an IBM Quantum Computer. *arXiv preprint arXiv:1711.09442* (2017).
61. Schuld, M., Fingerhuth, M. & Petruccione, F. Implementing a distance-based classifier with a quantum interference circuit. *Europhys. Lett.* **119**, 60002 (2017).
62. Sisodia, M. *et al.* Experimental realization of nondestructive discrimination of Bell states using a five-qubit quantum computer. *Phys. Lett. A* **381**, 3860–3874 (2017).
63. Tannu, S. S. & Qureshi, M. K. A Case for Variability-Aware Policies for NISQ-Era Quantum Computers. *arXiv preprint arXiv:1805.10224* (2018).
64. Wootton, J. R. Benchmarking of quantum processors with random circuits. *arXiv preprint arXiv:1806.02736* (2018).
65. Harper, R. & Flammia, S. Fault tolerance in the IBM Q Experience. *arXiv preprint arXiv:1806.02359* (2018).
66. Aggarwal, D., Raj, S., Behera, B. K. & Panigrahi, P. K. Application of quantum scrambling in Rydberg atom on IBM quantum computer. *arXiv preprint arXiv:1806.00781* (2018).
67. Srinivasan, K., Satyajit, S., Behera, B. K. & Panigrahi, P. K. Efficient quantum algorithm for solving travelling salesman problem: An IBM quantum experience. *arXiv preprint arXiv:1805.10928* (2017).



68. Dash, A., Sarmah, D., Behera, B. K. & Panigrahi, P. K. Exact search algorithm to factorize large biprimes and a triprime on IBM quantum computer. *arXiv preprint arXiv:1805.10478* (2018).
69. Roffe, J., Headley, D., Chancellor, N., Horsman, D. & Kendon, V. Protecting quantum memories using coherent parity check codes. *Quantum Sci. Technol.* **3**, 3 (2018).
70. Plesa, M.-I., & Mihai, T. A New Quantum Encryption Scheme. *Adv. J. Grad. Res.* **3**, 1 (2018).
71. Manabputra, Behera, B. K., & Panigrahi, P. K. A Simulational Model for Witnessing Quantum Effects of Gravity Using IBM Quantum Computer. *arXiv preprint arXiv:1806.10229* (2018).
72. Jha, R., Das, D., Dash, A., Jayaraman, S., Behera, B. K. & Panigrahi, P. K. A Novel Quantum N-Queens Solver Algorithm and its Simulation and Application to Satellite Communication Using IBM Quantum Experience. *arXiv preprint arXiv:1806.10221* (2018).
73. Gangopadhyay, S., Manabputra, Behera, B. K. & Panigrahi, P. K. Generalization and Demonstration of an Entanglement Based Deutsch-Jozsa Like Algorithm Using a 5-Qubit Quantum Computer. *Quantum Inf. Process.* **17**, 160 (2018).
74. Aggarwal, D., Raj, S., Behera, B. K. & Panigrahi, P. K. Application of quantum scrambling in Rydberg atom on IBM quantum computer. *arXiv preprint arXiv:1806.00781* (2018).
75. Warren, J. J., Winkler, J. R. & Gray, H. B. Hopping Maps for Photosynthetic Reaction Centers. *Cord. Chem. Rev.* **257**, 165–170 (2013).

76. Gilmore, J. & McKenzie, R. H. Spin boson models for quantum decoherence of electronic excitations of biomolecules and quantum dots in a solvent. *J. Phys. Condens. Matter* **17**, 1735 (2005).
77. Hussain, S. A. An Introduction to Fluorescence Resonance Energy Transfer *Sci. J. Phys.* **82**, 432–435 (2012).
78. Dacres, H., Wang, J., Dumancic, M. M. & Towell, S. C. Hopping Maps for Photosynthetic Reaction Centers. *Cord. Chem. Phys.* **82**, 432–435 (2013).
79. Hopfield, J. J. Electron Transfer Between Biological Molecules by Thermally Activated Tunneling. *Proc. Natl. Acad. Sci. USA* **71**, 3640–3644 (1974)
80. Wang, H. & Thoss, M. From coherent motion to localization: dynamics of the spin-boson model at zero temperature. *New J. Phys.* **10**, 115005 (2008).
81. Marcus, R. A. & Sutin, N. Electron transfers in chemistry and biology. *Biochim. Biophys. Acta Rev. Bioener.* **811**, 265–322 (1985).
82. Weiss, U., Grabert, H. & Linkwitz, S. Influence of friction and temperature on coherent quantum tunneling. *J. Low Temp. Phys.* **68**, 213–244 (1987).
83. Suarez, A. & Silbey, R. Properties of a macroscopic system as a thermal bath. *J. Chem. Phys.* **95**, 12 (1991).
84. Nielsen, M. A. & Chuang, I. L. Quantum Computation and Quantum Information (*Cambridge Univ. Press*, 2000).

85. Hegade, N. N, Behera, B. K. & Panigrahi, P. K. Experimental Demonstration of Quantum Tunneling in IBM Quantum Computer. *arXiv preprint arXiv:1712.07326* (2017)
86. Lloyd, S. Universal Quantum Simulators. *Science* **273**, 1073–1078 (1996).
87. Raeisi, S., Wiebe, S. & Sanders, B. C. Quantum-circuit design for efficient simulations of many-body quantum dynamics. *New J. Phys.* **14**, 103017 (2012).
88. Backend-information.  
<https://github.com/QISKit/qiskit-backend-information/tree/master/backends/tenerife/V1>

## Acknowledgements

The authors acknowledge Avinash Dash for useful dicussion; Daattavya Aggarwal and Deepankar Sarmah for helping in using QISKit. Y.M., D.S.A. and K.P. acknowledges the hospitality of Indian Institute of Science Education and Research Kolkata during the project work. Y.M. and B.K.B. acknowledge financial support of Inspire fellowship provided by Department of Science and Technology (DST), Govt. of India. We acknowledge the support of IBM Quantum Experience for providing access to the IBM quantum processors. The views expressed are those of the authors and do not reflect the official position of IBM or the IBM Quantum Experience team.

## Author contributions

The idea of simulating biological system by Spin-Boson Model was initially proposed by V.K. Theoretical analysis, design of quantum circuit simulation, collection and analysis of data were

performed by Y.M., D.S.A. and K.P. Y.M., D.S.A., K.P., V.K. and B.K.B. contributed to the composition of the manuscript. All authors have given approval to its final version. B.K.B. supervised the project. Y.M., D.S.A., K.P., V.K. and B.K.B. have completed the project under the guidance of P.K.P.

### **Competing interests**

The authors declare no competing financial interests. Readers are welcome to comment on the online version of the paper. Correspondence and requests for materials should be addressed to P.K.P. (pprasanta@iiserkol.ac.in).